Synchronization transitions on connectome graphs with external force

Géza Ódor, Istvan Papp, Shengfeng Deng
EK-MFA Complex Systems Department, Budapest
Jeffrey Kelling TUC, HZDR Dresden



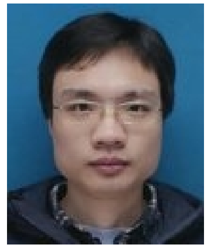


Synchronization transitions on connectome graphs with external force

Géza Ódor, Istvan Papp, Shengfeng Deng
EK-MFA Complex Systems Department, Budapest
Jeffrey Kelling TUC, HZDR Dresden



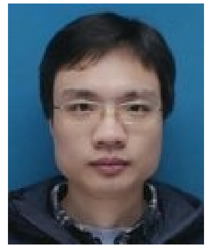


TECHNISCHE UNIVERSITÄT CHEMNITZ

Oscillatory behavior of neural systems +
Dynamical criticality in driven synchronization models ?

Synchronization transitions on connectome graphs with external force

Géza Ódor, Istvan Papp, Shengfeng Deng
EK-MFA Complex Systems Department, Budapest
Jeffrey Kelling TUC, HZDR Dresden



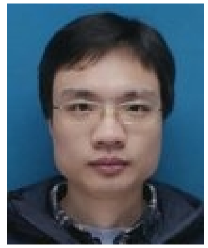


TECHNISCHE UNIVERSITÄT CHEMNITZ

Oscillatory behavior of neural systems +
Dynamical criticality in driven synchronization models ?
→ Community dependent, frustrated synchronization in brain **?**

Synchronization transitions on connectome graphs with external force

Géza Ódor, Istvan Papp, Shengfeng Deng
EK-MFA Complex Systems Department, Budapest
Jeffrey Kelling TUC, HZDR Dresden



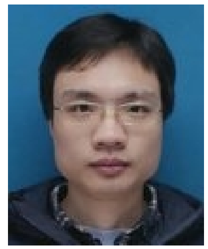


TECHNISCHE UNIVERSITÄT CHEMNITZ

Oscillatory behavior of neural systems +
Dynamical criticality in driven synchronization models ?
→ Community dependent, frustrated synchronization in brain **?**
Shinomoto-Kuramoto oscillator model synchronization transition:

$$\begin{aligned}\dot{\theta}_j(t) &= \omega_j^0 + K\sum_k W_{jk}\sin[\theta_k(t)-\theta_j(t)] \\ &+ F\sin(\theta_j(t)) + \epsilon\eta_j(t)\ .\end{aligned}$$

θ_i: angle, K: global coupling
F: external force, η_i: noise

Synchronization transitions on connectome graphs with external force

Géza Ódor, Istvan Papp, Shengfeng Deng
EK-MFA Complex Systems Department, Budapest
Jeffrey Kelling TUC, HZDR Dresden

  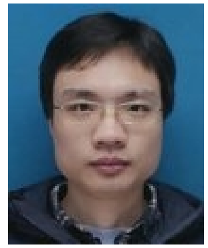 

TECHNISCHE UNIVERSITÄT CHEMNITZ

Oscillatory behavior of neural systems +
Dynamical criticality in driven synchronization models ?
→ Community dependent, frustrated synchronization in brain **?**
Shinomoto-Kuramoto oscillator model synchronization transition:

$$\dot{\theta}_j(t) = \omega_j^0 + K \sum_k W_{jk} \sin[\theta_k(t) - \theta_j(t)] + F \sin(\theta_j(t)) + \epsilon \eta_j(t) \ .$$

θ_i: angle, K: global coupling
F: external force, η_i: noise

Quenched heterogeneity in self-frequencies and network topology

Synchronization transitions on connectome graphs with external force

Géza Ódor, Istvan Papp, Shengfeng Deng
EK-MFA Complex Systems Department, Budapest
Jeffrey Kelling TUC, HZDR Dresden

  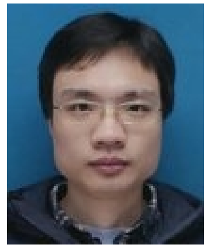 

TECHNISCHE UNIVERSITÄT CHEMNITZ

Oscillatory behavior of neural systems +
Dynamical criticality in driven synchronization models ?
→ Community dependent, frustrated synchronization in brain **?**
Shinomoto-Kuramoto oscillator model synchronization transition:

$$\dot{\theta}_j(t) = \omega_j^0 + K \sum_k W_{jk} \sin[\theta_k(t) - \theta_j(t)] + F \sin(\theta_j(t)) + \epsilon \eta_j(t) \ .$$

θ_i: angle, K: global coupling
F: external force, η_i: noise

Quenched heterogeneity in self-frequencies and network topology

Large Human Connectome graphs

Large Human Connectome graphs

Diffusion and structural MRI images with

$1\ mm^3$ voxel resolution :

$10^5 – 10^6$ nodes

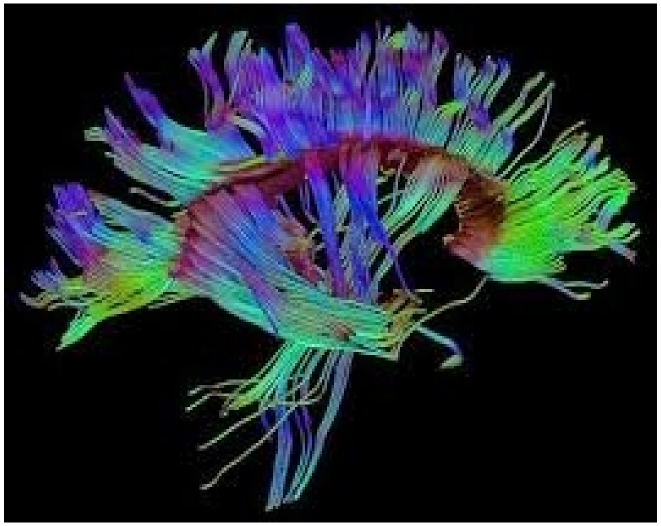

Large Human Connectome graphs

Diffusion and structural MRI images with

1 mm^3 voxel resolution :

$10^5 – 10^6$ nodes

Hierarchical modular graphs

Large Human Connectome graphs

Diffusion and structural MRI images with
1 mm^3 voxel resolution :
10^5 – 10^6 nodes

Hierarchical modular graphs

Top level: *70* brain region (Desikan atlas)

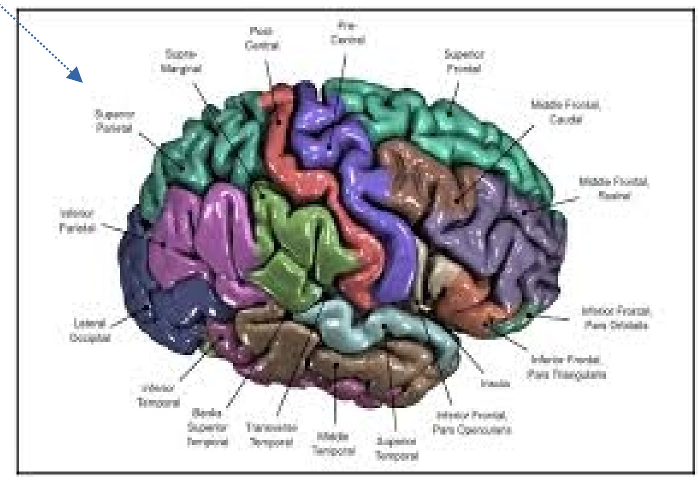

Large Human Connectome graphs

Diffusion and structural MRI images with
$1\ mm^3$ voxel resolution :
10^5 – 10^6 nodes

Hierarchical modular graphs

Top level: *70* brain region (Desikan atlas)

Lower levels obtained by deterministic tractography: FACT algorithm

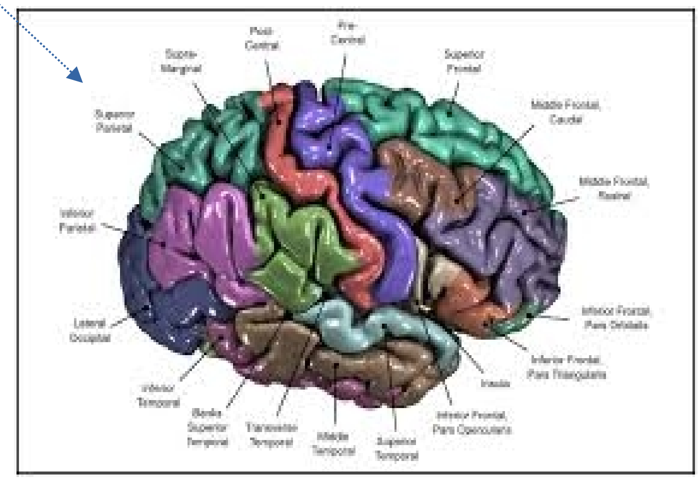

Large Human Connectome graphs

Diffusion and structural MRI images with
1 mm^3 voxel resolution :
10^5 – 10^6 nodes

Hierarchical modular graphs

Top level: *70* brain region (Desikan atlas)

Lower levels obtained by deterministic tractography: FACT algorithm

Map : voxel → vertex (~ 10^7)

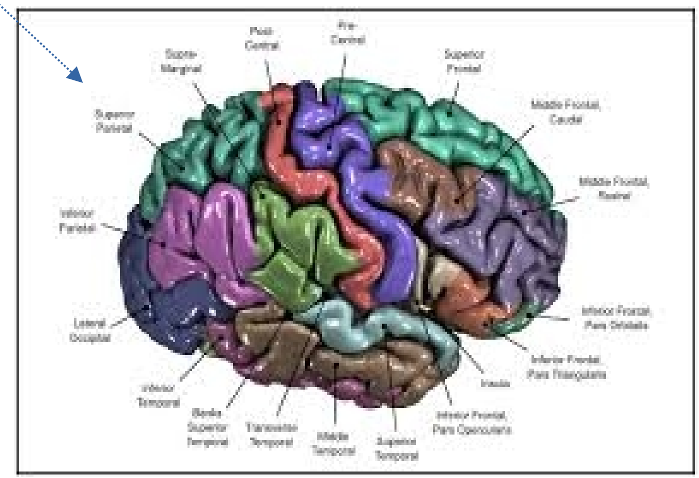

Large Human Connectome graphs

Diffusion and structural MRI images with
1 mm^3 voxel resolution :
$10^5 – 10^6$ nodes

Hierarchical modular graphs

Top level: *70* brain region (Desikan atlas)

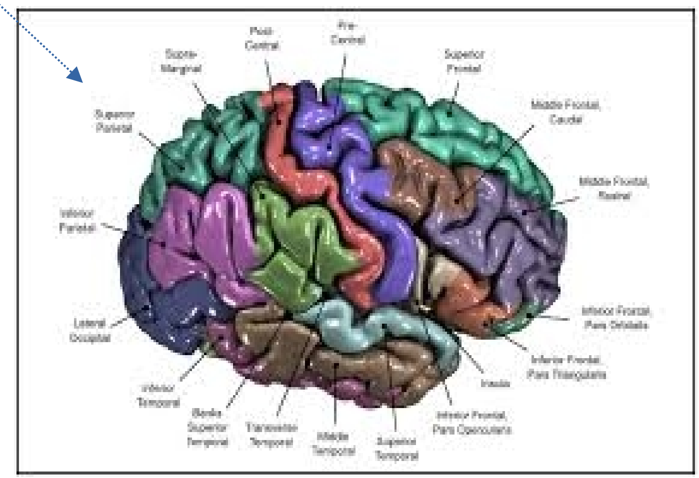

Lower levels obtained by deterministic
tractography: FACT algorithm

Map : voxel → vertex (~ 10^7)

fiber → edge (~ 10^{10})

Large Human Connectome graphs

Diffusion and structural MRI images with
1 mm^3 voxel resolution :
$10^5 – 10^6$ nodes

Hierarchical modular graphs

Top level: *70* brain region (Desikan atlas)

Lower levels obtained by deterministic tractography: FACT algorithm

Map : voxel → vertex (~ 10^7)

fiber → edge (~ 10^{10})

+ noise reduction → graph

undirected, weighted, *dim < 4 !*

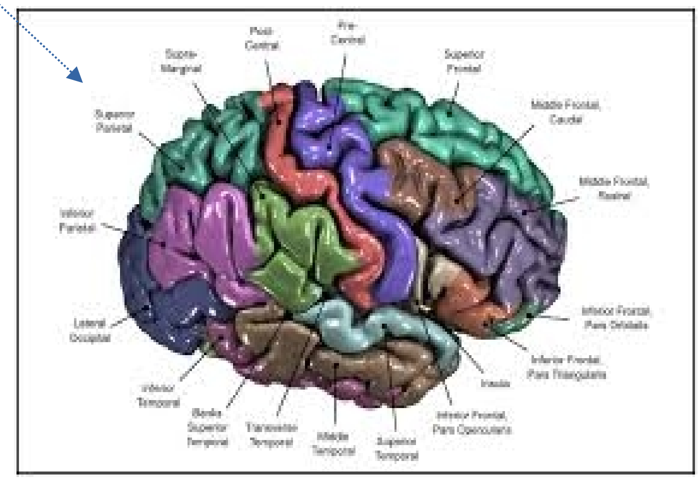

Large Human Connectome graphs

Diffusion and structural MRI images with
1 mm^3 voxel resolution :
10^5 – 10^6 nodes

Hierarchical modular graphs

Top level: *70* brain region (Desikan atlas)

Lower levels obtained by deterministic tractography: FACT algorithm

Map : voxel $\rightarrow$ vertex ($\sim 10^7$)

fiber $\rightarrow$ edge ($\sim 10^{10}$)

+ noise reduction $\rightarrow$ graph

undirected, weighted, *dim < 4 !*

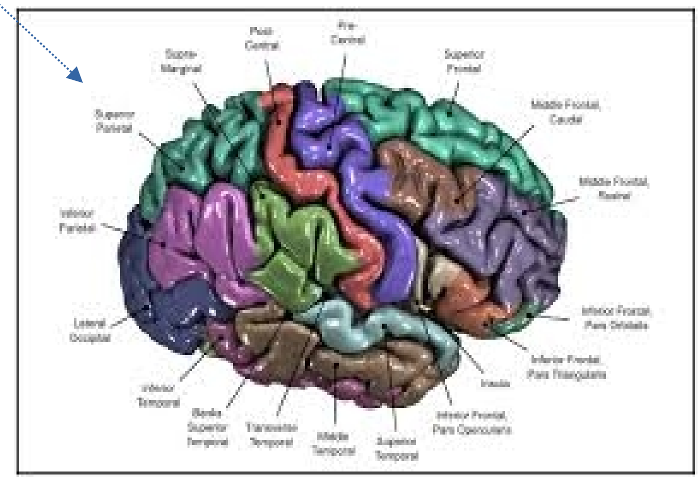

Structural graphs of nodes (containing ~10^4 neurons) and power-law weight distributed edges see : *Michael T. Gastner and Géza Ódor, Scientific Reports 6 (2016) 27249*

Comparison with the fruit-fly connecome results

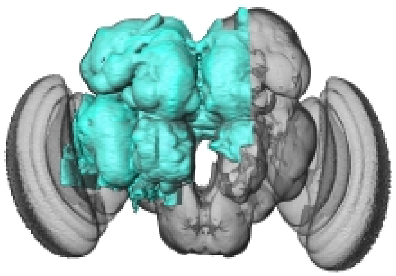

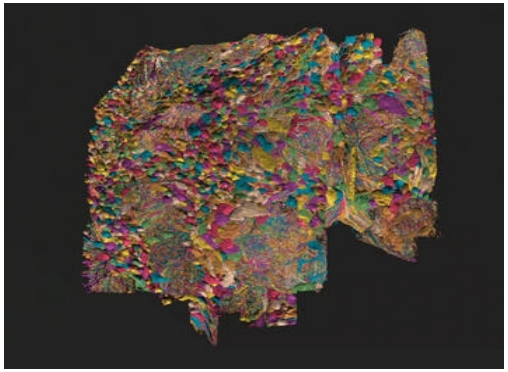

A_{ij}

Comparison with the fruit-fly connecome results

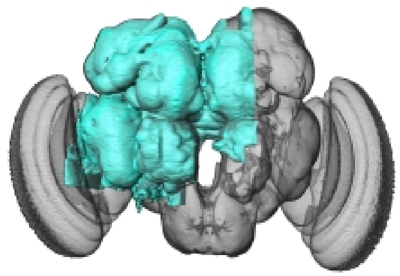

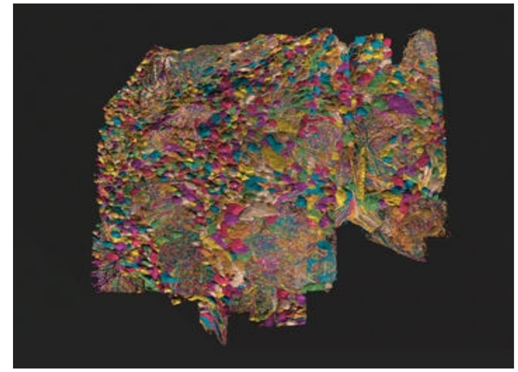

A_{ij}

The fruit-fly connectome is the largest exactly known neural network:
$N = 21.615$, $L = 3.410.247$, dim > 5, small world

Comparison with the fruit-fly connecome results

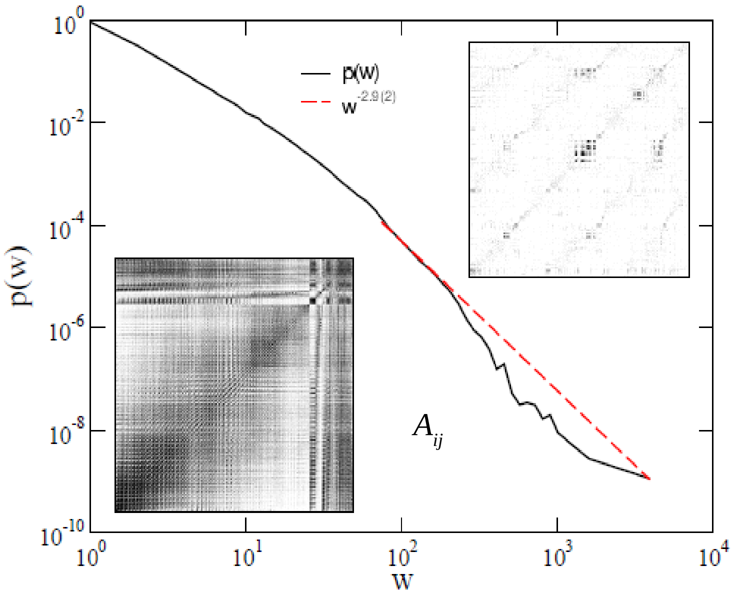

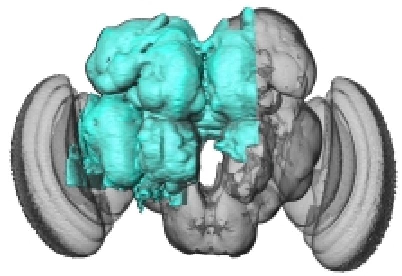

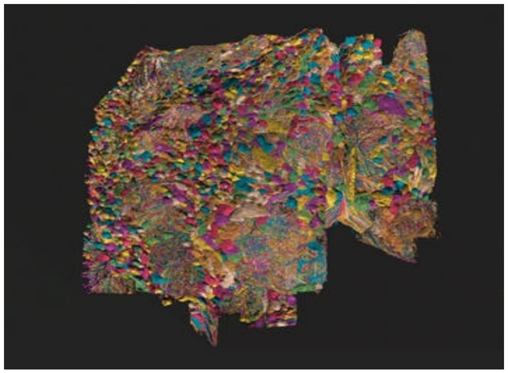

The fruit-fly connectome is the largest exactly known neural network:
N = 21.615, L = 3.410.247, dim > 5, small world

Similar to random Erdős-Rényi (random) graph, but power-law tailed connection weights

Comparison with the fruit-fly connecome results

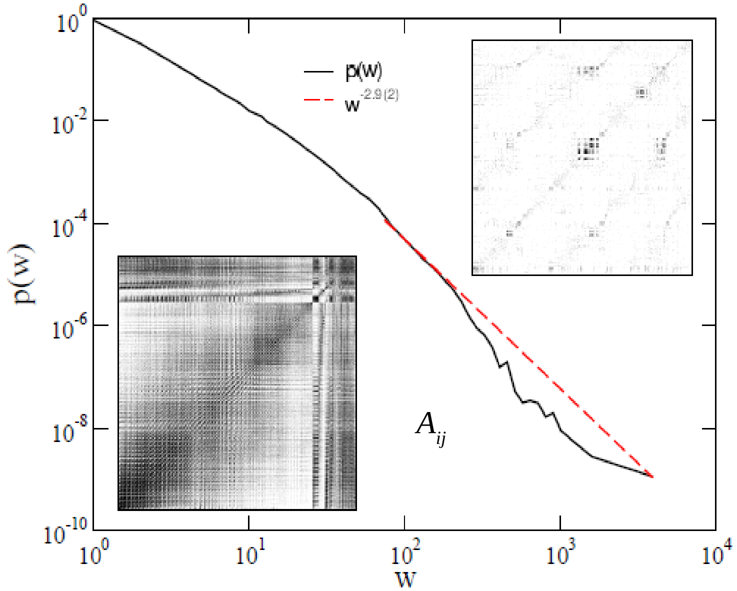

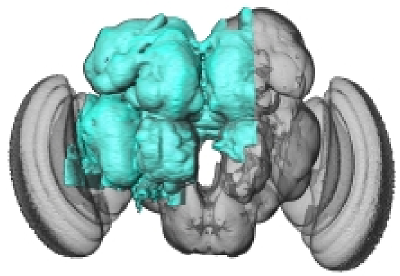

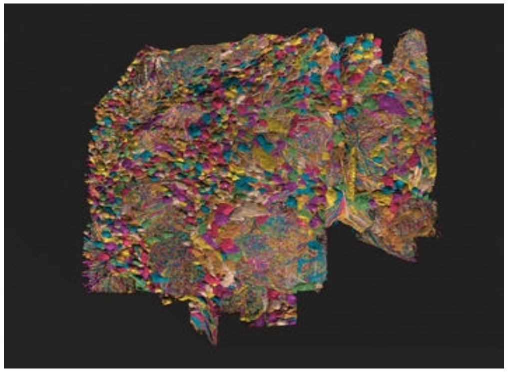

The fruit-fly connectome is the largest exactly known neural network:
N = 21.615, L = 3.410.247, dim > 5, small world

Similar to random Erdős-Rényi (random) graph, but power-law tailed connection weights

Weakly modular: $Q_{FF} = 0.63 \leftrightarrow Q_{KKI\text{-}18} = 0.91$

Comparison with the fruit-fly connecome results

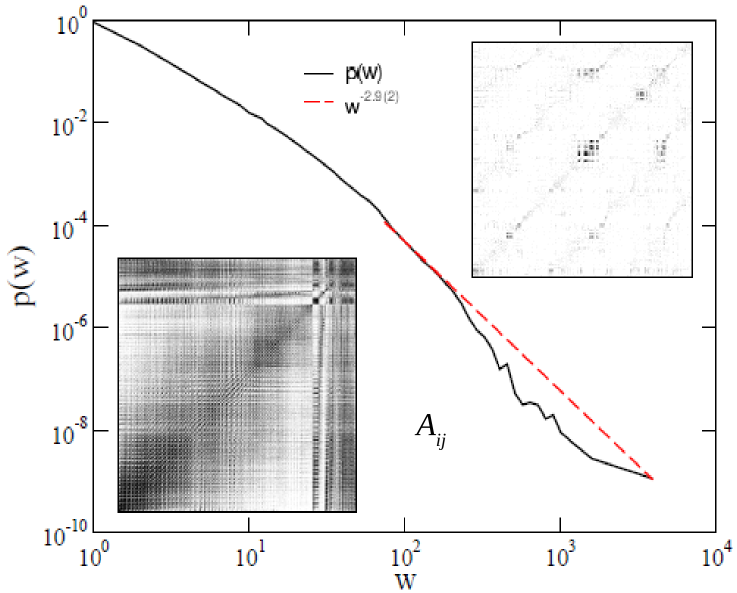

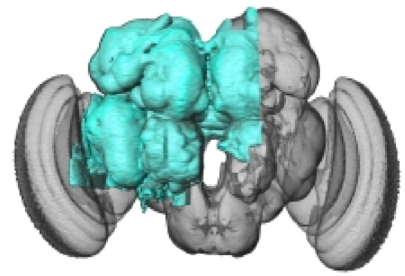

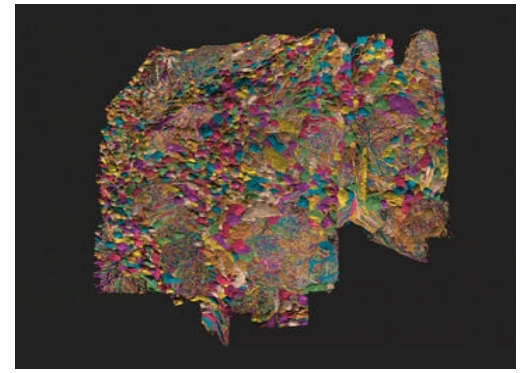

The fruit-fly connectome is the largest exactly known neural network:
N = 21.615, L = 3.410.247, dim > 5, small world

Similar to random Erdős-Rényi (random) graph, but power-law tailed connection weights

Weakly modular: $Q_{FF} = 0.63 \leftrightarrow Q_{KKI\text{-}18} = 0.91$

Modeling inhibition via weight renormalization :

$$W'_{jk} = W_{jk} / \sum_k W_{jk}$$

Numerical integration of the model

Numerical integration of the model

Global synchronization measures:

Numerical integration of the model

Global synchronization measures: $r(t) \exp i\theta(t) = 1/N \sum_j \exp\left[i\theta_j(t)\right]$

Numerical integration of the model

Global synchronization measures:

$$r(t)\exp i\theta(t) = 1/N\sum_j \exp\left[i\theta_j(t)\right]$$

$$R(t) = \langle r(t)\rangle$$

Numerical integration of the model

Global synchronization measures: $r(t)\exp i\theta(t) = 1/N \sum_j \exp\left[i\theta_j(t)\right]$

$$R(t) = \langle r(t) \rangle \qquad \Omega(t) = \frac{1}{N}\sum_{j=1}^{N}(\overline{\omega}(t) - \omega_j^2(t))$$

Numerical integration of the model

Global synchronization measures: $$r(t)\exp i\theta(t) = 1/N\sum_j \exp\left[i\theta_j(t)\right]$$

$$R(t) = \langle r(t)\rangle \qquad \Omega(t) = \frac{1}{N}\sum_{j=1}^{N}(\overline{\omega}(t) - \omega_j^2(t))$$

Local synchronization measures:

Numerical integration of the model

Global synchronization measures:

$$r(t)\exp i\theta(t) = 1/N\sum_j \exp\left[i\theta_j(t)\right]$$

$$R(t) = \langle r(t)\rangle$$

$$\Omega(t) = \frac{1}{N}\sum_{j=1}^{N}(\overline{\omega}(t) - \omega_j^2(t))$$

Local synchronization measures:

$$R_i(t) = \frac{1}{N_{\mathrm{i.neigh}}}\left|\sum_j^{N_{\mathrm{i.neigh}}} A_{ij}e^{i\theta_j(t)}\right|$$

Numerical integration of the model

Global synchronization measures:

$$r(t)\exp i\theta(t) = 1/N\sum_j \exp\left[i\theta_j(t)\right]$$

$$R(t) = \langle r(t)\rangle$$

$$\Omega(t) = \frac{1}{N}\sum_{j=1}^{N}(\overline{\omega}(t) - \omega_j^2(t))$$

Local synchronization measures:

$$R_i(t) = \frac{1}{N_{\text{i.neigh}}}\left|\sum_j^{N_{\text{i.neigh}}} A_{ij}e^{i\theta_j(t)}\right|$$

$$\Omega_i(t) = \frac{1}{N_{\text{i.neigh}}}\left|\sum_j^{N_{\text{i.neigh}}} (\overline{\omega}(t) - \omega_j(t))^2\right|$$

Numerical integration of the model

Global synchronization measures:

$$r(t)\exp i\theta(t) = 1/N \sum_j \exp\left[i\theta_j(t)\right]$$

$$R(t) = \langle r(t) \rangle$$

$$\Omega(t) = \frac{1}{N}\sum_{j=1}^{N}(\overline{\omega}(t) - \omega_j^2(t))$$

Local synchronization measures:

$$R_i(t) = \frac{1}{N_{\text{i.neigh}}}\left|\sum_j^{N_{\text{i.neigh}}} A_{ij} e^{i\theta_j(t)}\right|$$

$$\Omega_i(t) = \frac{1}{N_{\text{i.neigh}}}\left|\sum_j^{N_{\text{i.neigh}}} (\overline{\omega}(t) - \omega_j(t))^2\right|$$

Hurst (phase) and beta exponent analysis of local order parameters

Numerical integration of the model

Global synchronization measures:

$$r(t)\exp i\theta(t) = 1/N \sum_j \exp\left[i\theta_j(t)\right]$$

$$R(t) = \langle r(t) \rangle$$

$$\Omega(t) = \frac{1}{N}\sum_{j=1}^{N}(\overline{\omega}(t) - \omega_j^2(t))$$

Local synchronization measures:

$$R_i(t) = \frac{1}{N_{\text{i.neigh}}}\left|\sum_j^{N_{\text{i.neigh}}} A_{ij}e^{i\theta_j(t)}\right|$$

$$\Omega_i(t) = \frac{1}{N_{\text{i.neigh}}}\left|\sum_j^{N_{\text{i.neigh}}} (\overline{\omega}(t) - \omega_j(t))^2\right|$$

Hurst (phase) and beta exponent analysis of local order parameters

$$\mathbb{E}\left[\frac{Z(n)}{S(n)}\right] = Cn^H$$

Numerical integration of the model

Global synchronization measures:

$$r(t) \exp i\theta(t) = 1/N \sum_j \exp\left[i\theta_j(t)\right]$$

$$R(t) = \langle r(t) \rangle$$

$$\Omega(t) = \frac{1}{N} \sum_{j=1}^{N} (\overline{\omega}(t) - \omega_j^2(t))$$

Local synchronization measures:

$$R_i(t) = \frac{1}{N_{\text{i.neigh}}} \left| \sum_j^{N_{\text{i.neigh}}} A_{ij} e^{i\theta_j(t)} \right|$$

$$\Omega_i(t) = \frac{1}{N_{\text{i.neigh}}} \left| \sum_j^{N_{\text{i.neigh}}} (\overline{\omega}(t) - \omega_j(t))^2 \right|$$

Hurst (phase) and beta exponent analysis of local order parameters

$$\mathbb{E}\left[\frac{Z(n)}{S(n)}\right] = Cn^H$$

$$S(f) = \left| \sum_{j=0}^{N} \Omega_j(t) e^{-2\pi i f_j / N} \right|^2 \approx 1/f^\beta$$

Numerical integration of the model

Global synchronization measures:

$$r(t)\exp i\theta(t) = 1/N\sum_j \exp\left[i\theta_j(t)\right]$$

$$R(t) = \langle r(t)\rangle \qquad \Omega(t) = \frac{1}{N}\sum_{j=1}^{N}(\overline{\omega}(t) - \omega_j^2(t))$$

Local synchronization measures:

$$R_i(t) = \frac{1}{N_{\text{i.neigh}}}\left|\sum_j^{N_{\text{i.neigh}}} A_{ij}e^{i\theta_j(t)}\right| \qquad \Omega_i(t) = \frac{1}{N_{\text{i.neigh}}}\left|\sum_j^{N_{\text{i.neigh}}} (\overline{\omega}(t) - \omega_j(t))^2\right|$$

Hurst (phase) and beta exponent analysis of local order parameters

$$\mathbb{E}\left[\frac{Z(n)}{S(n)}\right] = Cn^H \qquad S(f) = \left|\sum_{j=0}^{N}\Omega_j(t)e^{-2\pi i f_j/N}\right|^2 \approx 1/f^\beta$$

Numerical ODE solution of large set of equations via adaptive

Bulrisch-Stoer stepper, implemented on HPC GPU-s

Implementation on GPU-s

- C++
- VexCL github.com/ddemidov/vexcl
  - library for parallel execution of vector expressions via CUDA, OpenCL or OpenMP
  - support for custom kernels (but no abstraction)
- `boost::numeric::odeint` odeint.com
  - template library of ODE solvers
  - supports VexCL as backend
  - using Runge−Kutta 4, Bulirsch−Stoer, Euler−Maruyama (SDE, custom)
- Counter-based RNG: Philox [4]
  - implemented by VexCL
  - exact reproducibility of noise across platforms / devices
- ADIOS 2 adios2.readthedocs.io
  - for fast, self-describing I/O

Performance

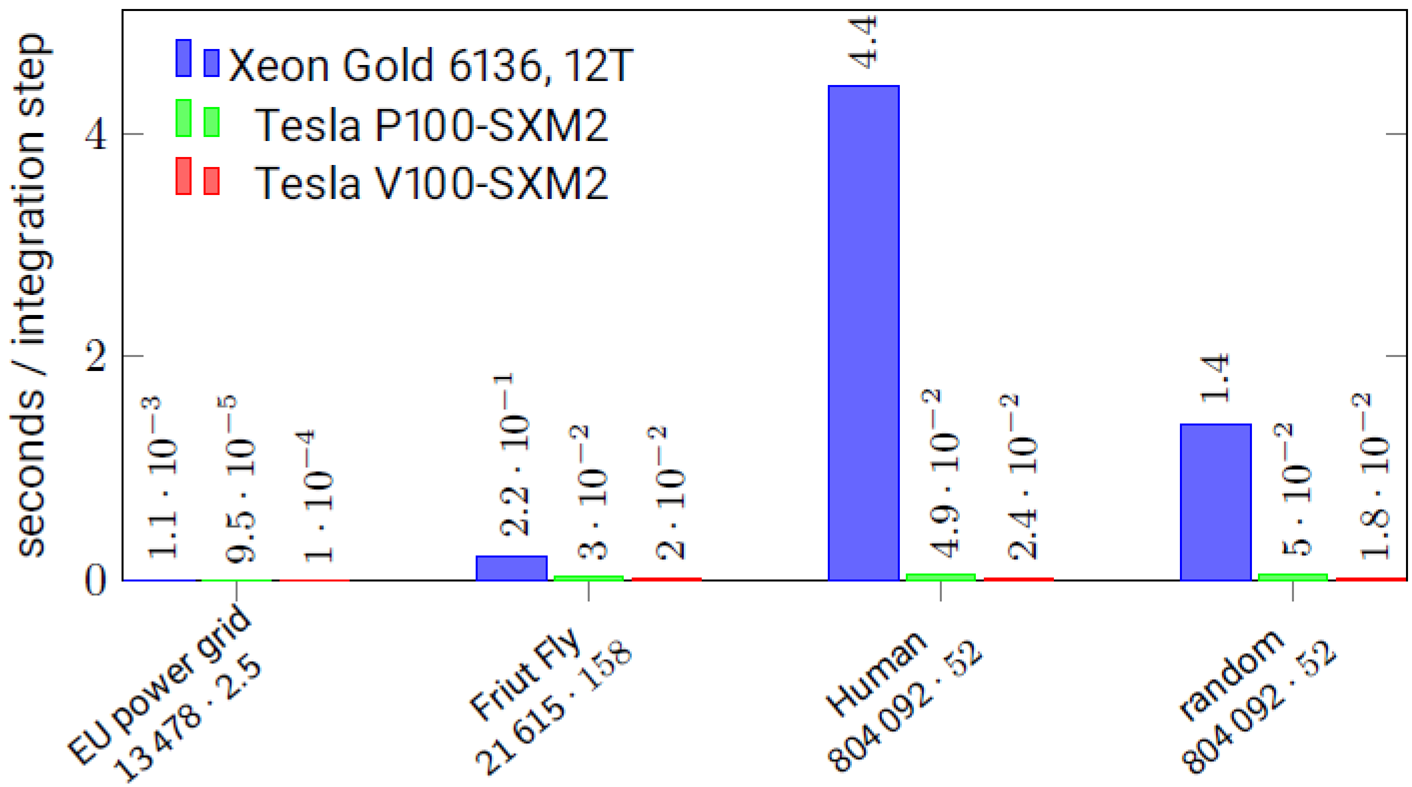

Performance

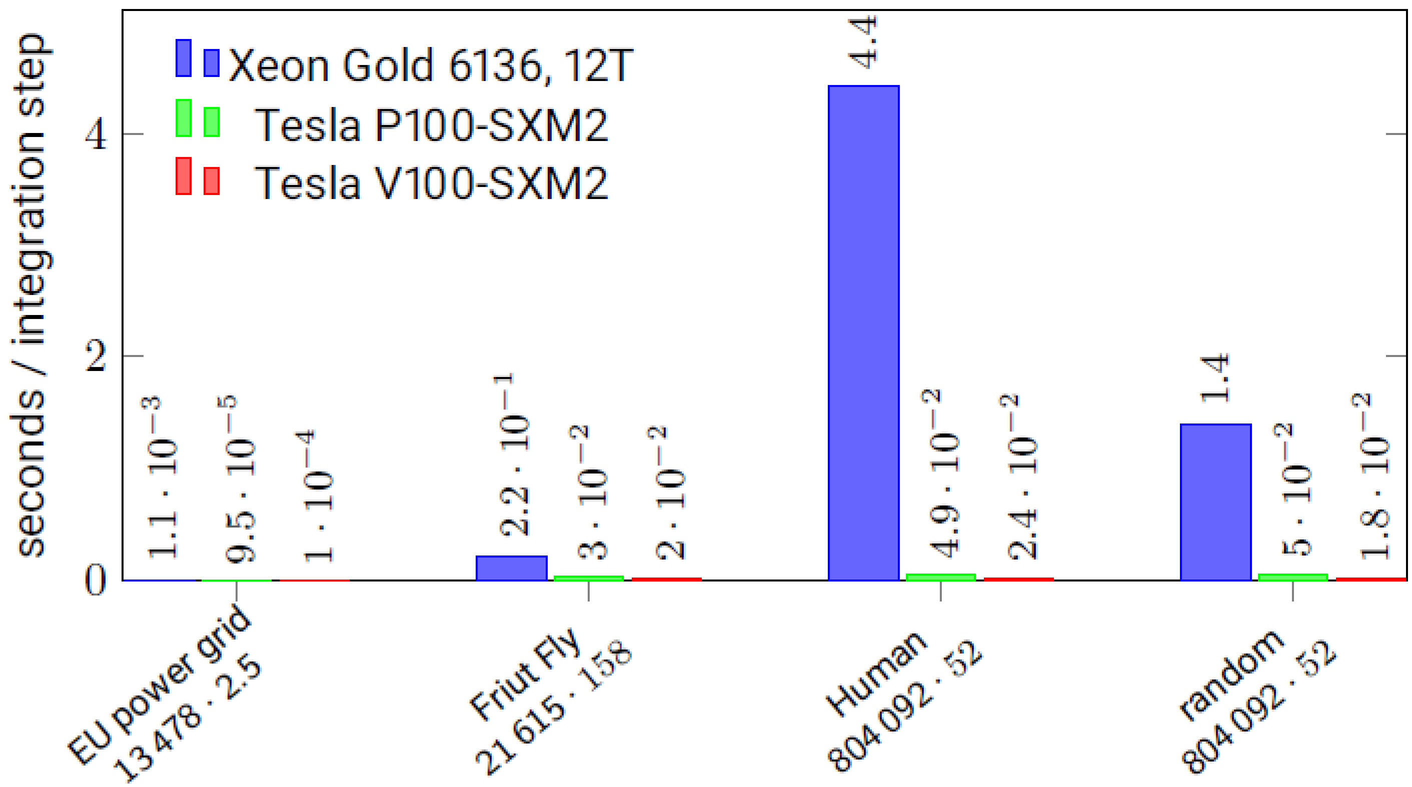

Benchmark on Komondor (A100) ↔ Leo (K40),

Speedup ~*3x* in case of the fly, ~*6x* in case of the human connectome

Force induced synchronization

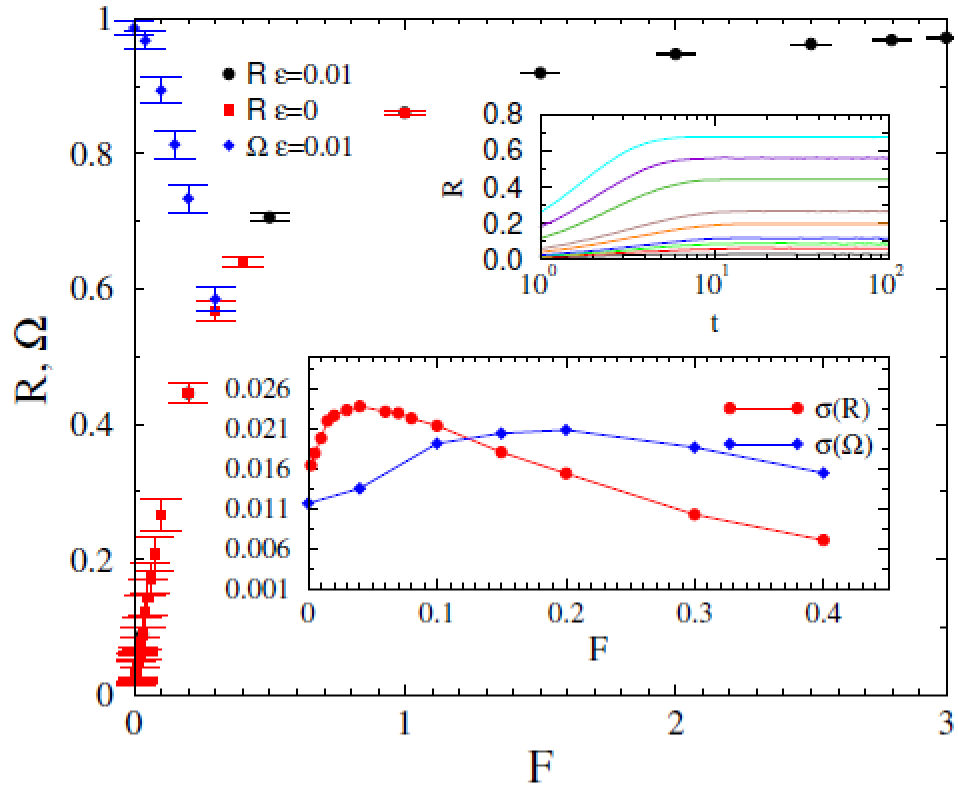

FIG. 1: Order parameter dependence on F for the fruit-fly connectome for the noisy (black bullet) and the noiseless (red boxes) cases at $K = 1.3$. The blue diamonds show the steady-state Ω values with noise. Lower inset: Variances of R and Ω for the noisy case. Upper inset: Time dependence of the noisy $R(t)$, for $F = 0, 0.02, 0.03, 0.04, 0.07, 0.1, 0.2, 0.3, 0.4$ (bottom to top curves).

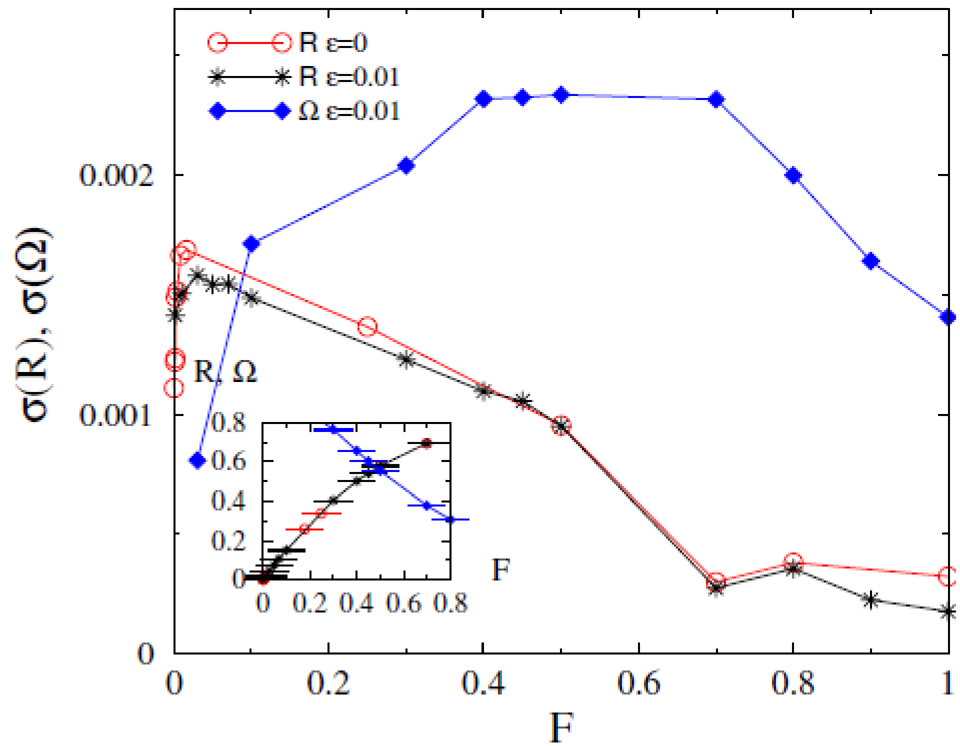

FIG. 3: Fluctuations of R and Ω as the function of F for the KKI-18, for the noisy and the noiseless cases at $K = 1$. Inset: Order parameter R for the noisy and noiseless cases as well as Ω, denoted by the same symbols as in the main figure.

Characteristic time exponent τ_t results

Characteristic time exponent τ_t results

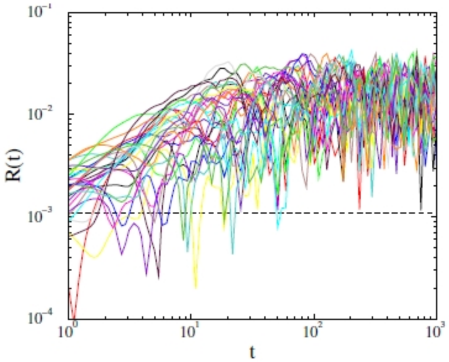

Characteristic time exponent τ_t results

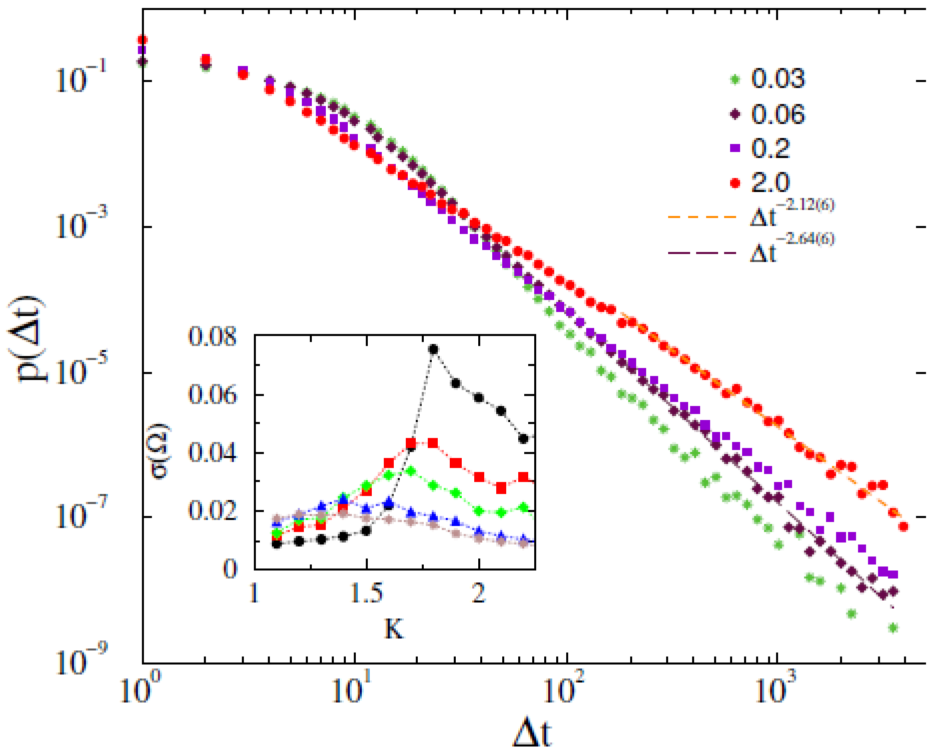

FIG. 4: Avalanche duration distributions on the fruit-fly connectome for different forces, shown by the legends and at $K = 1.3$, $\epsilon = 0.01$. Dashed lines are PL fits for $\Delta t > 100$. The inset shows the steady state $\sigma(\Omega)$ as the function of K, for excitation values $F = 0.001, 0.0667, 0.1, 0.2, 0.3$ (top to bottom).

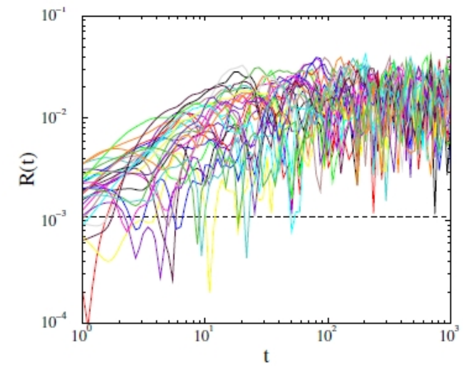

The $p(t_x)$ distros exhibit power-law near the synchronization transition point $F_c \sim 0.1$ for $K=1.3$ characterized by the exponent: *2*

Characteristic time exponent τ_t results

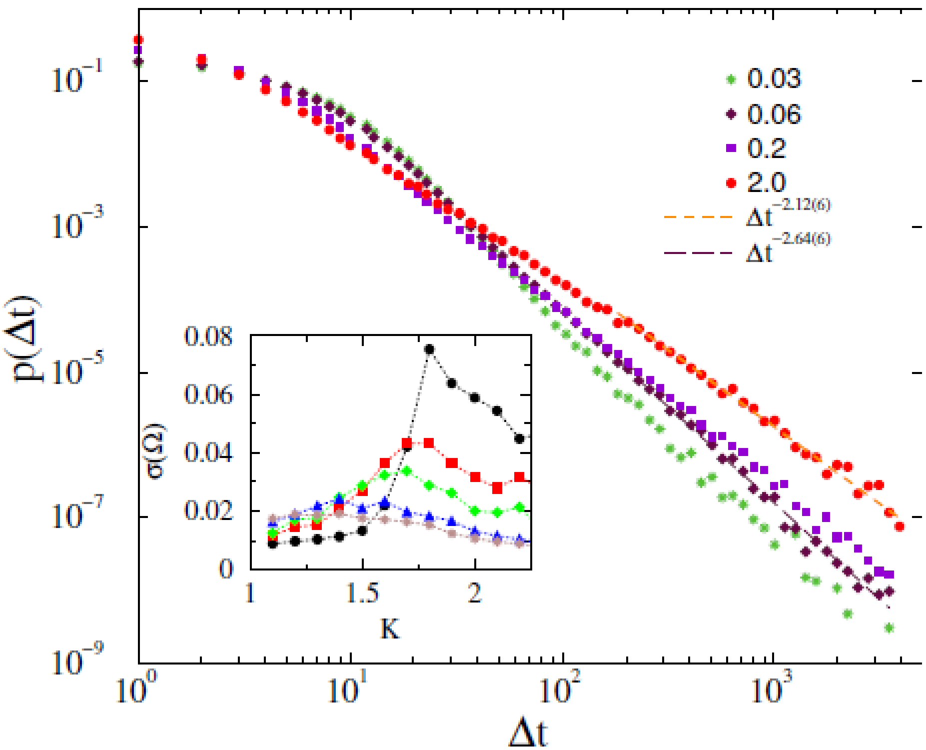

FIG. 4: Avalanche duration distributions on the fruit-fly connectome for different forces, shown by the legends and at $K = 1.3$, $\epsilon = 0.01$. Dashed lines are PL fits for $\Delta t > 100$. The inset shows the steady state $\sigma(\Omega)$ as the function of K, for excitation values $F = 0.001$, 0.0667, 0.1, 0.2, 0.3 (top to bottom).

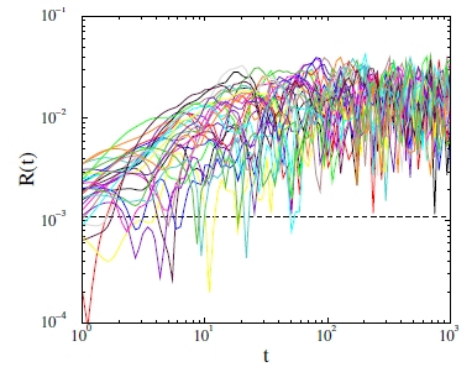

The $p(t_x)$ distros exhibit power-law near the synchronization transition point $F_c \sim 0.1$ for $K=1.3$ characterized by the *exponent: 2*

Similarly as in case of the KKI-18:

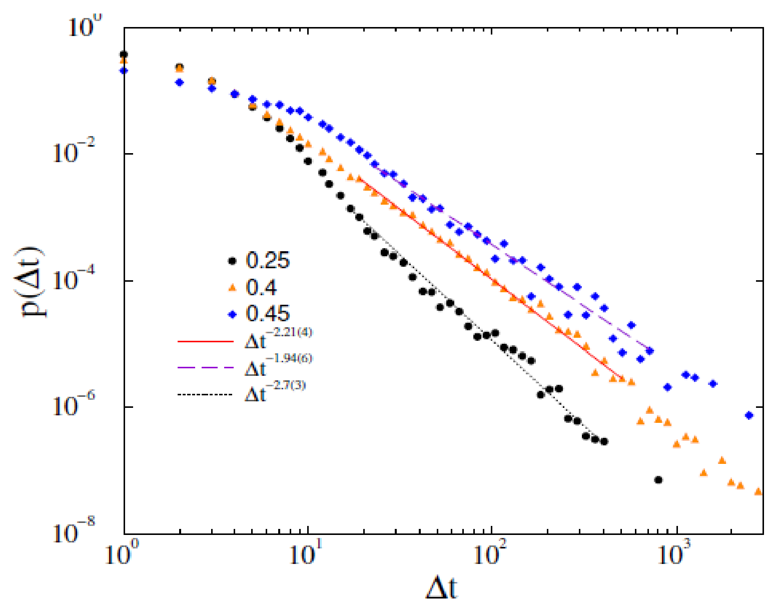

Local order parameter of the fly

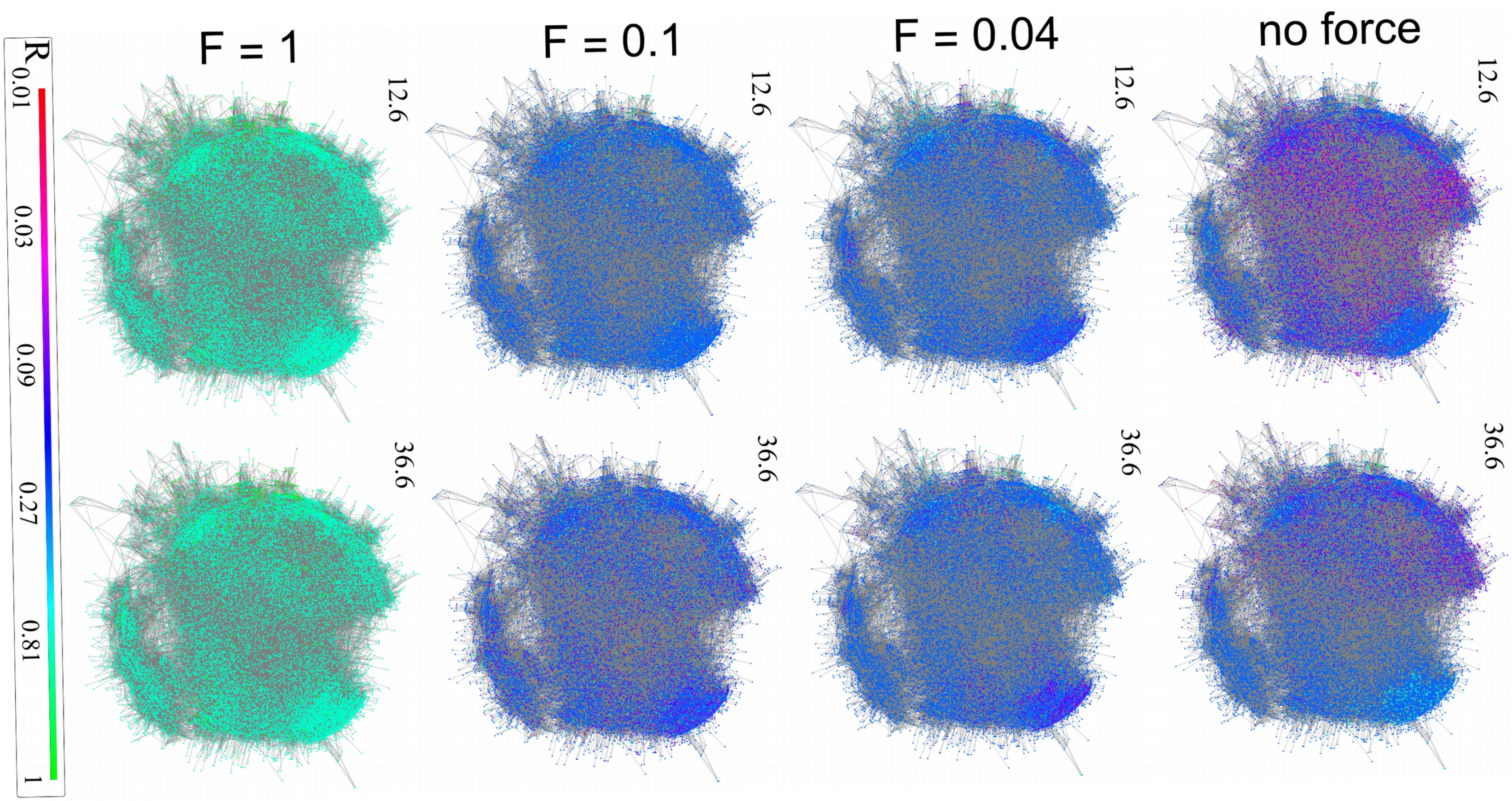

Frustrated synchronization (in domains), Chimera states

Hurst and beta exponent analysis

Hurst and beta exponent analysis

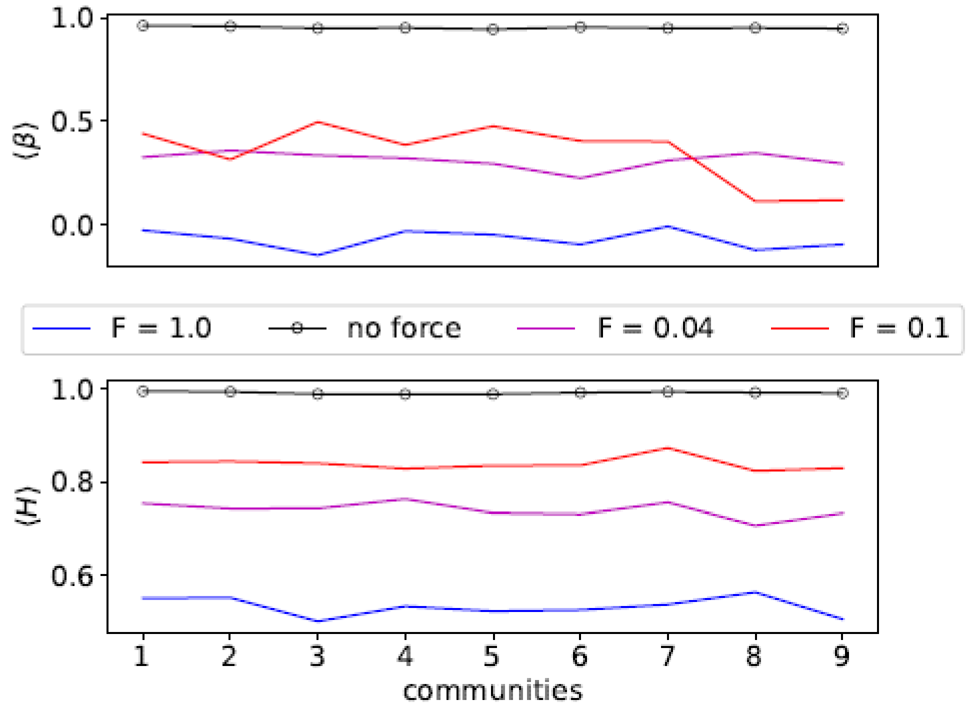

FIG. 8: Hurst and beta exponents of all fruit-fly connectome communities. In the forceless case at the critical Hopf transition coupling, the H exponent is the largest for every community. With forces these values drop for each community. This shows a resemblance with the rest and non-rest studies of different brain areas in [63], showing $\langle H \rangle \approx 1.0$ at resting state and $\langle H \rangle \approx 0.7$ at task driven states.

Hurst and beta exponent analysis

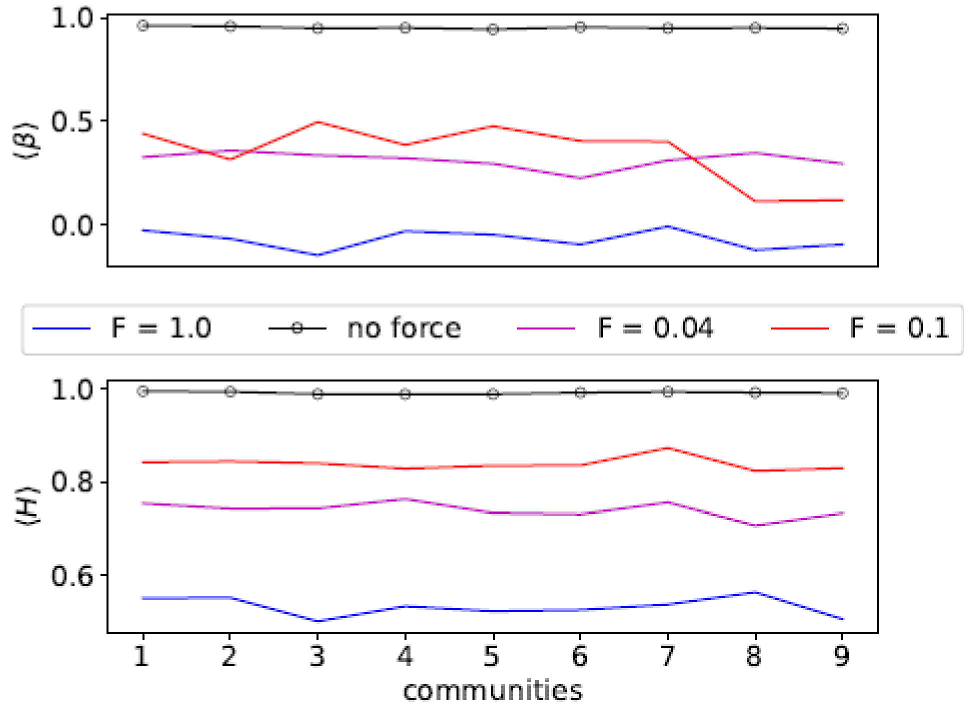

FIG. 8: Hurst and beta exponents of all fruit-fly connectome communities. In the forceless case at the critical Hopf transition coupling, the H exponent is the largest for every community. With forces these values drop for each community. This shows a resemblance with the rest and non-rest studies of different brain areas in [63], showing $\langle H \rangle \approx 1.0$ at resting state and $\langle H \rangle \approx 0.7$ at task driven states.

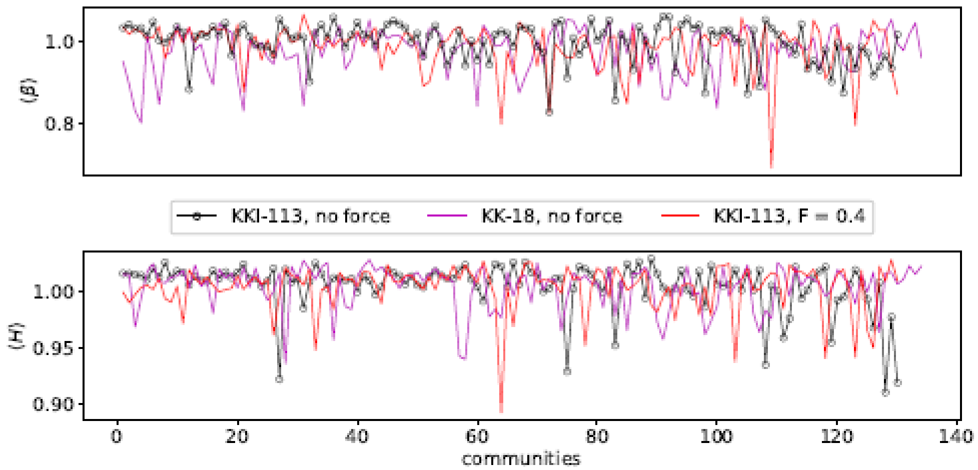

FIG. 9: Hurst and β exponents of all human connectomes' communities. KKI-113 is presented with and without force terms and KK-18 without the force terms.

Hurst and beta exponent analysis

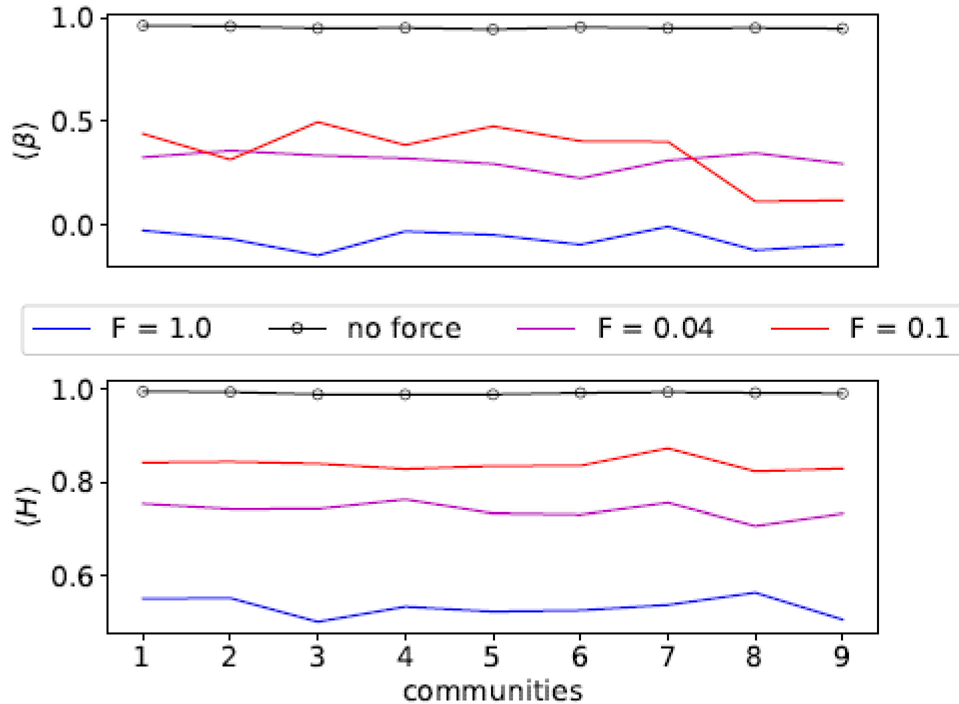

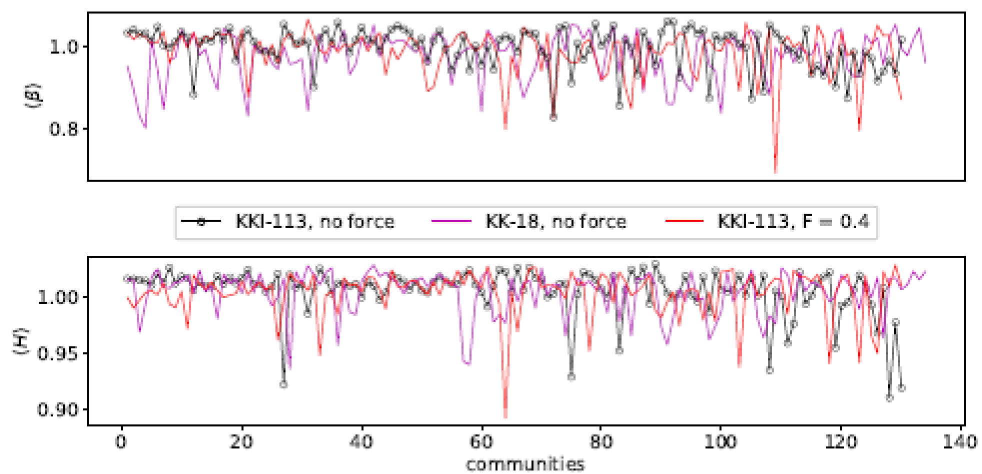

FIG. 9: Hurst and β exponents of all human connectomes' communities. KKI-113 is presented with and without force terms and KK-18 without the force terms.

FIG. 8: Hurst and beta exponents of all fruit-fly connectome communities. In the forceless case at the critical Hopf transition coupling, the H exponent is the largest for every community. With forces these values drop for each community. This shows a resemblance with the rest and non-rest studies of different brain areas in [63], showing $\langle H\rangle \approx 1.0$ at resting state and $\langle H\rangle \approx 0.7$ at task driven states.

Community dependent synch.

Quasi-criticality, like in fMRI

experiments: *Ochab et al*,

Sci. Rep. 12, 17866 (2022).

FMRI experiments

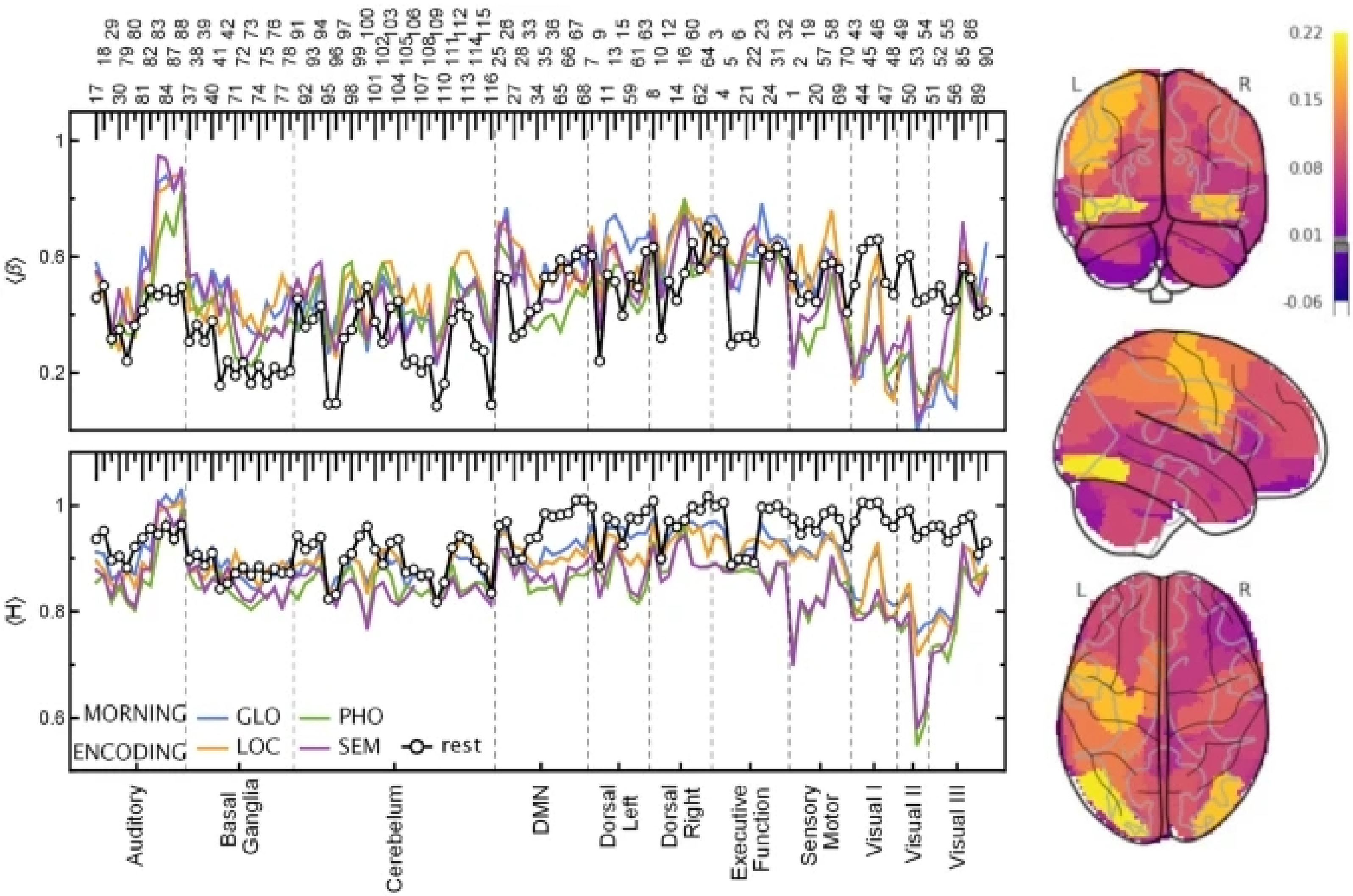

Task ↔ rest state operation

Conclusions

Conclusions

- Periodic external force induces synchronization transition in Kuramoto type models applied on fruit-fly and human connectome graphs

Conclusions

- Periodic external force induces synchronization transition in Kuramoto type models applied on fruit-fly and human connectome graphs
- Local synchronization analysis reveals Chimera states Hurst and beta exponents in communities show quasi-criticality in agreement with fMRI experiments:

Conclusions

- Periodic external force induces synchronization transition in Kuramoto type models applied on fruit-fly and human connectome graphs
- Local synchronization analysis reveals Chimera states Hurst and beta exponents in communities show quasi-criticality in agreement with fMRI experiments:
- Force enhances long-range correlations, i.e. in the task phase operation of brain with respect to resting state

Conclusions

- Periodic external force induces synchronization transition in Kuramoto type models applied on fruit-fly and human connectome graphs
- Local synchronization analysis reveals Chimera states Hurst and beta exponents in communities show quasi-criticality in agreement with fMRI experiments:
- Force enhances long-range correlations, i.e. in the task phase operation of brain with respect to resting state
- Thank you for the attention !

Géza Ódor, Istvan Papp, Shengfeng Deng and Jeffrey Kelling :
Synchronization transitions on connectome graphs with external force
Front. Phys. 11 (2023) 1150246.

Géza Ódor, Gustavo Deco and Jeffrey Kelling
Differences in the critical dynamics underlying the human and fruit-fly connectome
Phys. Rev. Res. 4 (2022) 023057.